Detecting aerofoil separation pre-cursors using on-board optical tracking of flexible pillar sensors

Omar Selim (omar.selim@city.ac.uk)
City, University of London
Christoph Bruecker
City, University of London

Research Article

Keywords: Aerodynamic separation, bio-inspired, flow sensor, UAV

Posted Date: November 8th, 2022

DOI: https://doi.org/10.21203/rs.3.rs-2222213/v1

Additional Declarations: No competing interests reported.

Detecting aerofoil separation pre-cursors using on-board optical tracking of flexible pillar sensors

Omar Selim and Christoph Bruecker†

Department of Mechanical Engineering and Aeronautics, City, University of London, London, EC1V 0HB, United Kingdom.

Contributing authors: omar.selim@city.ac.uk; christoph.bruecker@city.ac.uk;
†These authors contributed equally to this work.

Abstract

A novel approach for detecting characteristic flow signatures precursory to stall along aerofoils is introduced. It uses arrays of flexible wind-hair like sensors distributed around the aerofoil which are tracked remotely using high-speed imaging and processing. The sensors act as "digital tufts" providing real-time readings of local velocity information with a high temporal resolution. Such sensors are integrated into a NACA0012 aerofoil and tested in a wind-tunnel for varying angles of attack in static tests and dynamically in a ramp-up test. For the static tests, the mean values of the sensor signals provide information on local free-stream velocity and angle of incidence. The fluctuating part of the signals show that at angles approaching separation prominent low frequency oscillations are detected, the magnitudes of which scale with the angle of incidence. These are hypothesised to be linked to breathing modes of the Laminar Separation Bubble causing a shear-layer flapping observed on the sensors. Such low-frequency oscillations were also detected short before separation in the ramp-up studies. As the high-speed cameras are mounted in a simulated "on-board" position, the sensing method could be used for early stall warnings in small-scale UAVs with integrated on-board object tracking cameras.

Keywords: Aerodynamic separation, bio-inspired, flow sensor, UAV

1 Introduction

With the introduction of small and medium UAV's into every day commercial and non-commercial operations, the effects of flow separation and subsequent loss of lift at low to mid-range Reynold's numbers are becoming more and more impactful. At best, these effects can reduce the power-efficiency of an aircraft, shifting the flight out of the optimal conditions, which requires consistent, drag-costly alterations of flight attitude to return to optimal flight, and at worst these effects can result in eventual catastrophic failures and loss of the system entirely. Thus, the early prediction of flow separation by monitoring the emergence of any pre-cursory signals indicating the state of incipient separation is becoming ever-more important to ensure safe and efficient operation of these systems. Such signals should best be a primary representation of the velocity profiles and the pressure distribution along the wing with high spatial and temporal resolution. The latter however requires larger preparation costs of the wing, can be applied only at specific locations and require onboard instrumentation. Often a compromise of number of sensors is required for practical applications. In addition, the pressure signal alone is not able to predict a local flow separation. Therefore, sensors detecting the current state of the near-wall velocity profile in the boundary layer are highly demanded.

The detection and response to temporal changes in flow of varying frequency ranges is nothing new to natural fliers. Investigations of biological inspired sensors have shown a variety of natural fliers using wing receptors to detect temporal flow and pressure changes, in addition to variations of amplitude for signals of the same frequency for executive decision making in flight control and stabilisation[1]. Even in high-speed flight, mechanoreceptors on fast-fliers have the ability to scale with flow conditions to a high level of sensitivity [2], which is critical during high-speed stoops where small changes to angle of attack can have significant effects on lift generation and flight stability [3].

Inspired from nature, wind-hair receptors were explored in [4] for detecting changes in the boundary layer velocity profiles giving detailed information of the overall flow conditions. When those sensors are exposed to flow they show a deflection response as a result of the length-integrated load distribution along the filamentous hairs. Their response was tested under different shape factors of the velocity profile and for different boundary layer thicknesses and they concluded that such wind-hairs are sensitive to flow profile changes from favourable to adverse pressure gradients. Micro-pillar shear stress sensors are even able to sense directly the velocity gradient at the wall [5] and such can be used to detect local flow reversals [6]. Their mechanical behavior is well defined under static and dynamic load conditions, therefore the sensors can quantify the wall-shear stress in magnitude and direction. This however limits the size of those sensors in practical applications to the scale of the viscous boundary layer which is typically in the sub-millimeter range. For practical application, larger "wind-hairs" could be a compromise between gain in sensitivity (stronger bending forces) while losing spatial resolution due to the wall-normal integration effect.

The present work uses bio-inspired wind-hairs in the form of flexible cantilever structures on a NACA0012 aerofoil. The tips of these are tracked by an object tracking camera placed in a simulated "on-board" position along the span of the wing section. It aims to detect characteristic fluctuations of the velocity profile that are correlating to flow phenomena unique to those angles of attack which are incipient to flow separation. Such correlations are known to exist from previous CFD simulations and TR-PIV measurement on a NACA0012 aerofoil undergoing stall. It has been shown [7] how, at moderate to high pre-stall angles of attack, breathing modes of the laminar separation bubble existing on the suction side of a NACA0012 can trigger shear layer separation resulting in quasi-periodic oscillations in lift and drag. This is further validated with LES simulations in which they have shown the presence of this separation bubble and how the frequency of oscillation changes at angles of incidence approaching stall. Further experimental work on investigating the presence, cause, and effect of these oscillations were carried out by [8] where TR-PIV was carried out over a NACA0012 aerofoil at various pre-stall angles of attack. There, wavelet analysis was carried out in addition to smoke visualisation experiments showing the low-frequency oscillations who's frequency increased with angle of attack at the onset of stall. Such a signature of onset of stall is aimed to be tested with the developed system herein.

2 Experimental Arrangement

2.1 Aerofoil preparation

The design and manufacturing of the pillar sensors follows the concept described in earlier work [9] using flexible micro-pillars to detect and characterise wall shear stress in the aortic artery. The sensors were scaled up to match the scales and application of the current investigation to act as 'digital tufts' over the wing surface.

The aerofoil model used is a constant NACA0012 aerofoil of chord length 0.19m and span of 0.70m. It is assembled from segments of 3D printed NACA-0012 sections with a Perspex centre section to provide optical access through the mid-span location (Fig. 2). These sections are clamped together with the sheet of pillars placed in-between at one side of the transparent segment. The sheet is made from a silicone film (thickness $2mm$, density $1.2g/cm^3$, Young's modulus E = $2.45MPa$) that is the base of the pillars and is laser-cut to the outer contour of the aerofoil. At the outer edge arrays of pillars in the shape of rectangular beams were left out (height 7.2mm, width 0.37mm). When the sheet is clamped between the 3D printed section and the perspex section (Fig. 2) it is flush with the surface while the pillars protrude into the flow at a right angle to the local surface. The pillar tips and specific marker points along the chord are labelled with florescent dye (MMA-RhB-Frak-Paticles, Dantec

Dynamics, peak emission at 584 nm, peak absorption at 540 nm) and illuminated with an LED illuminator. Thus, using optical lens filters as wavelength separation of the emitted light, the tips can be isolated from the surrounding background. The so prepared aerofoil with integrated bio-inspired flexible pillar sensors is shown in (Fig. 2).

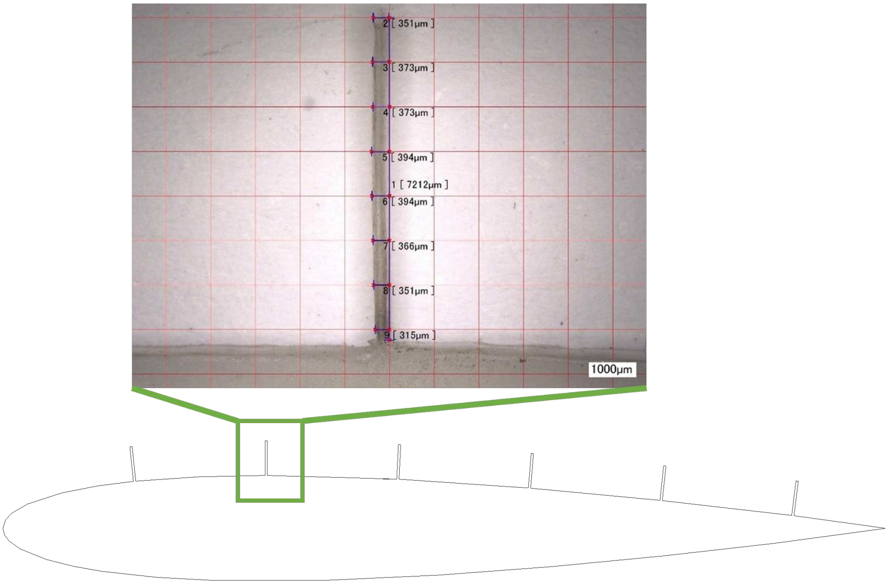

Fig. 1: Magnified image of one of the pillar sensors under a 200x microscope lens showing the details of the structure and pertinent dimensions. The pillars are numbered in the following from no.1 at the uppermost left to 6 at the most downstream one near the trailing edge.

2.2 Wind-tunnel setup

The model is placed in the T2 tunnel of the Handley-Page lab at City, University of London. This is a closed-loop wind tunnel with a turbulence intensity of 0.8 %. The test section is 0.81m x 1.22m where the model is mounted such that one end of the aerofoil spans to the floor while the free end is fitted with an end plate to negate tip effects. Optical access is achieved through one transparent side window and the bottom which is used to illuminate the sensor tips and record their tip-motion. Supportive flow measurements were done with a Time-Resolved PIV system which was arranged with the light sheet in the plane of the pillars. The experimental setup for the PIV system can be seen in (Fig. 3). A Phantom M310 camera was arranged orthogonally to the laser sheet and fitted with 100mm lens. A Litron LDY300 dual-head laser was used to illuminate the measurement plane. Seeding is done using DEHS tracer

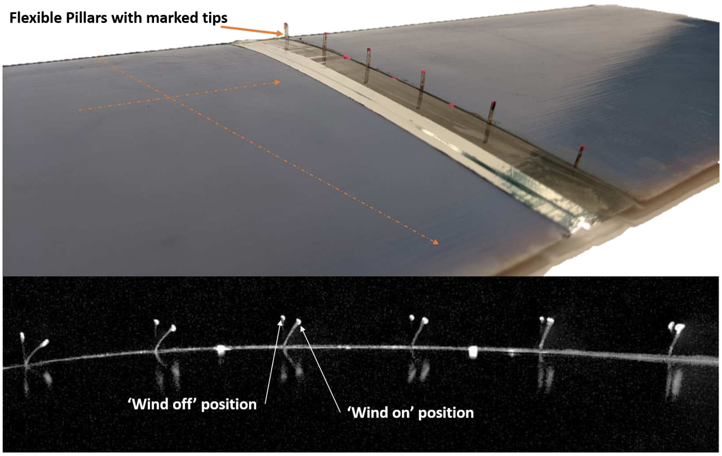

Fig. 2: Top: Image from 'wing-root' position showing the different components of the model; in blue are the 3D printed aerofoil sections, and between is a transparent Perspex section, also showing the flexible pillars emanating from the surface, which could be extended to a full 'skin' with 2D arrays of sensors. Bottom: Overlain images from the object tracking camera in the simulated 'on-board' position showing sample pillar deflections. (flow is left to right)

particles injected into the flow in the settling chamber upstream of the wind tunnel nozzle. Insight V3V-4G software was used to coordinate the laser pulses and image capture at a repetition rate of 1kHz and laser pulse separation of 30 microseconds. A standard multi-pass cross-correlation algorithm is applied to process the image pairs and analyse the flow field.

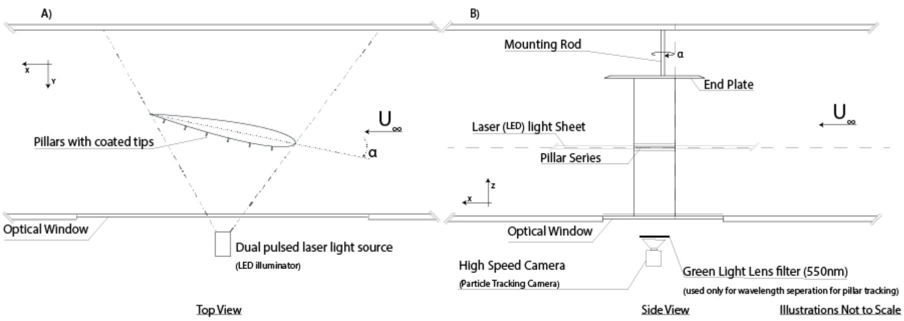

Fig. 3: Experimental arrangement for the wind-tunnel studies. LED light source and Laser illumination were interchangeable with minimal disruption. Text between brackets indicates the alternative arrangement for the different experiments. A: top view, B: front view

2.3 Optical sensor tracking

The signal detection process is the optical tracking of the sensor tip displacement Q(t), which is proportional to the bending moment imposed by the flow-induced drag forces. This is measured by comparing the location of the tip in wind-on with wind-off situation. In the following we consider Q as only the tangential component in the sensor plane (parallel to the wall). A high-speed camera (ProcImage 500-Eagle high-speed camera, 1280 px × 1024 px, Photon Lines Ltd, Bloxham, UK) is mounted outside the tunnel along the span-wise line of the wing, to simulate where an on-board camera would be mounted, and fitted with a green light lens filter (long-pass optical filter, cut-on wavelength of 550nm, Edmund Optics), thus only receiving the light emission from the fluorescent labelled pillar tips (and marker points). From this position the camera captures the pillar tip positions at a sampling rate of 500 Hz in two different modes; standard mode, seen in (Fig. 2) fitted with a 50mm lens, and binary mode with centroid detection of white connected pixels at a selected area in the frame, which outputs a stream of coordinate points with a time-marker corresponding to 6 pillar tips and 2 marker points. Using a 100mm lens a finer resolution can be obtained over 3 pillars of interest to allow more spatial resolution recordings. This method of data acquisition was also used to acquire position data for underwater artificial seal whiskers [10]. Such an object tracking camera can provide a quasi on-line response of the flow state around the aerofoil by tracking the sensors. Additionally, using a Phantom M310, the same recordings were captured and the positions of those tips are then found using a MATLAB based code similar to PIV, where a small interrogation window around the tip is cross-correlated between images of wind-on and wind-off situation. This serves the purpose of validating the results from the tracking, and as a proof of concept for further work assembling pillars with an on-board cameras in-situ on an airborne UAV.

2.4 Sensor calibration

In order to characterise the static and dynamic response of the pillars mechanical tests and FEA simulations were carried out and compared. From a mechanical point of view, the pillars act as one-sided clamped cantilevered beams of nearly uniform rectangular cross-section, (see Fig. 1). The static deflection of the sensors was tested when exposed to a wall-jet like flow with approximately constant velocity over the pillar length. Using a correlation of the drag force for a cylinder, subsequent finite element simulations were carried out aimed to analyse the sensitivity of pillar tip deflection to these variations in loading. Measurement data for a cylinder within the experimental range of Reynolds numbers were taken from [11] and approximated with a power-fit for the drag coefficient in the following form ($R^2 = 0.967$):

$$C_d = 3.0244 \times Re^{-0.155} \tag{1}$$

The calibration flow is generated with a small and handy open-ended wind-tunnel with one-sided contraction nozzle at the exit (lenght 75cm, nozzle width W=12cm, nozzle height H=10mm, contraction ratio 10:1) fashioned at the facilities in order to carry out in-situ calibration of the pillar sensors at the most upstream pillar near the leading edge, see (Fig.4). Flow is driven by a set of four fans at the inlet of the tunnel and exits the nozzle with the bottom wall flush aligned tangential to the upper section of the suction side, thus producing a near constant velocity along the pillar. Flow velocities at the pillar locations were measured with a hotwire anemometer. The results show only little variation of velocity over the length of the pillar, thus for the FEA simulation the velocity along the pillar is assumed to be constant in first approximation.

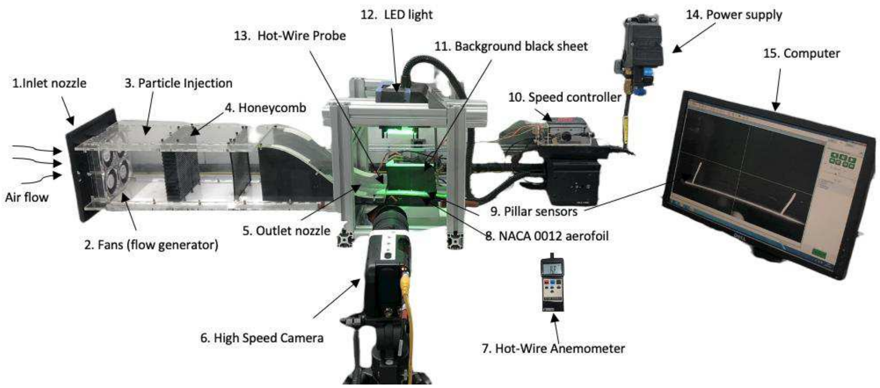

Fig. 4: Experimental setup of the wall-jet for sensor calibration, showing different components for various calibration related tests.

3 Results and Discussion

3.1 Calibration

The results from the calibration of the leading pillar no.1 are most significant to obtain an understanding of free-stream velocity. This pillar is located at 15% chord – thus experiencing the least effects of boundary layer thickness which, at its largest, is approximately 10% of the entire pillar length. In addition, as seen from equation 3 the contribution of the very near-wall flow to the total moment in equilibrium with the elastic restoring forces is of second order. Thus, the tip deflection Q(t), which is dictated by the moment balance about the clamped end of the beam, can provide a reliable source of information on free-stream velocity. The effects of angle of attack on the deflection of the first pillar are investigated further later in this section. The instantaneous load distribution g(t,l) acting normal to the longitudinal axis of the pillar is derived in analogy to work from [9].

$$g(t,l) = q_\infty(l,t) \times b \times C_d(Re_l) \tag{2}$$

$$M(t) = \int_0^l g(t,l) \times l \, dl \tag{3}$$

The results from the experimental calibration of the leading edge pillar are shown in Fig. 5 labeled as "Experiment". A good agreement is found with the FEA simulation for the load distributions corresponding to the same velocities within the experiment. Because of growing instabilities from the outer shear-layer of the wall-jet, reliable steady flows with constant velocity at the pillar could only be achieved up to free-stream velocities of 10m/s. This is where the simulations help to extend the calibration curve to higher velocities as those expected in the experiments at the largest Re-numbers. As the tip deflection goes beyond 30% of the pillar length L, the reconfiguration of the pillar get considered large. The effect of reconfiguration can be seen in (Fig. 5) where an increase in velocity results in less of an increase of deflection at velocities higher than approx. 12 m/s above which the Cauchy number is larger than unity, see [12]. In general, flexible elements have a natural tendency to modulate the total drag force experienced by reconfiguration.

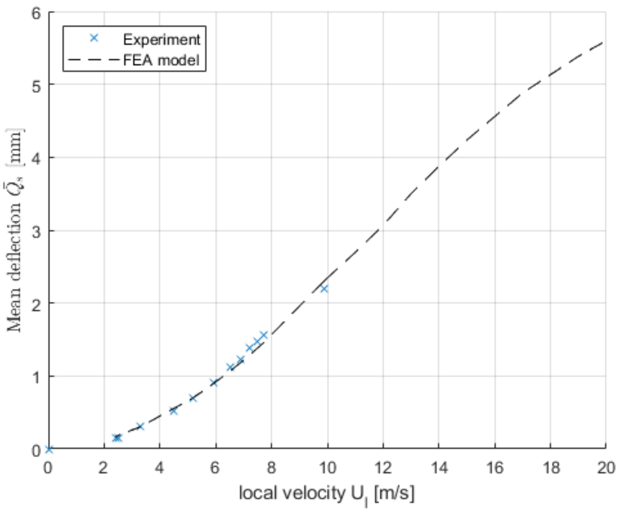

Fig. 5: Tip deflection of pillar no.1 measured against the results from the FEA simulation with variation of wall-jet velocity. Symbols: measurements with the wall-jet facility; dashed line: simulations.

Moreover, the dynamic response of the sensors was obtained from a step-response test in-situ, where the optical setup was the same as the wind tunnel experiments but with no flow. The pillars were deflected to an initial position and then released, leading to a damped oscillatory motion back to the resting position as plotted in Fig. 7. The natural frequency is estimated from the plot to be approximately 59 Hz which is in good agreement with the FEA simulation of the 1st bending mode (corresponding to the natural frequency in vacuum situation with no damping).Higher order bending and torsional twist are also estimated from the simulations and occur only at about 7-8 times higher frequencies, which are not of relevance for the current moderate Re-number flows. Similarly, flutter is only happening at excitation frequencies higher than 230Hz as calculated according to [13].

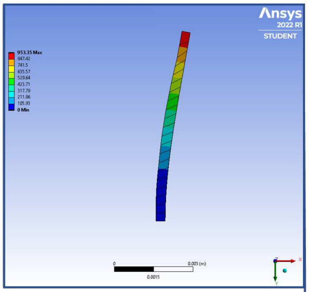

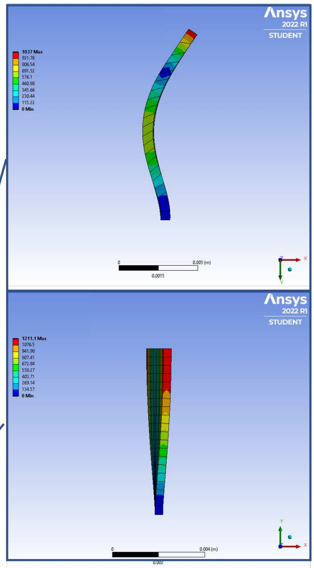

Mode	Freq [Hz]
1^{st} bending (Exp)	58.9
1^{st} bending (FEA)	56.8
2^{nd} bending (FEA)	347.16
1^{st} torsional (FEA)	445.64

Fig. 6: Structural modes of the sensor and corresponding onset frequencies.

With the given data of static and dynamic response, the postprocessing of the data was tailored to recover only the low-frequency content of the pillar motion using a low-pass filter with a cut-off frequency of $20Hz$. This ensures on one hand high-enough temporal resolution for the expected low-frequency oscillations related to incipient stall while it removes noise from self-excited vibrations or small-scale turbulent structures. Additionally, the range of free-stream velocities tested herein is below those that would send the pillars into flutter. Higher Reynolds number flows correspond with larger reconfigurations, which also means that vortex induced vibrations effects are limited [14].

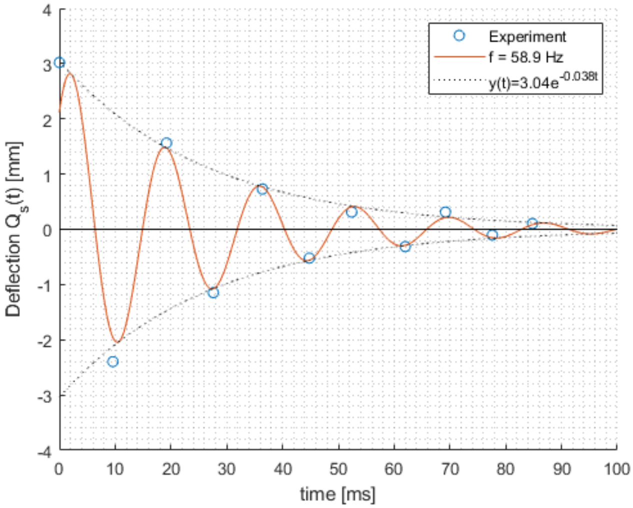

Fig. 7: Response of the flexible pillar when released from forced bend to free relaxation back to its resting position. Symbols: measurements at the peak tip excursions; solid line: fit with a damped harmonic oscillation at natural frequency of 58.9Hz; dashed line: fit to the amplitude dampening function.

3.2 Aerofoil experiment

The wind tunnel experiments with the prepared aerofoil were carried out at varying angles of attack and at a free-stream velocity of $15m/s$ corresponding to a Reynolds number of 200,000. Pillar motion tracking was done at a sampling rate of 500 Hz.

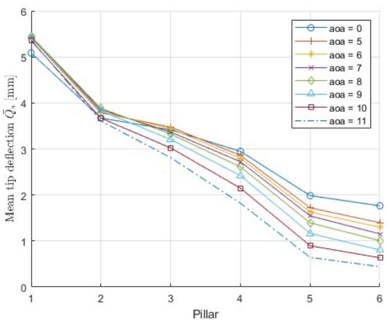

(a)

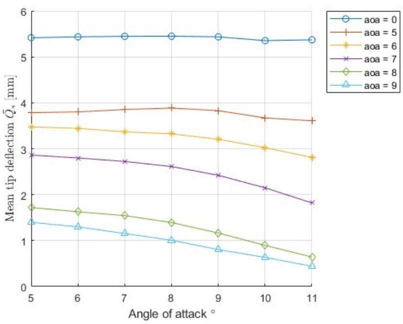

(b)

Fig. 8: Mean tip deflection $\overline{Q_s}$ at different sensor positions along the chord (a) and for varying angle of attack (b).

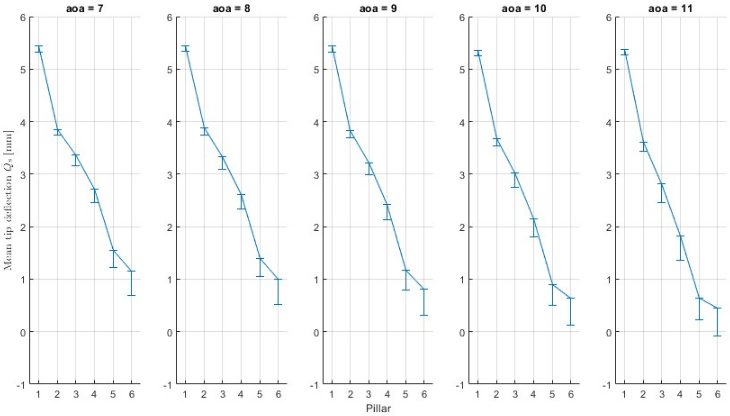

Fig. 9: Mean deflection and range of negative fluctuating excursions (against mean flow direction) for each pillar for moderate, pre-stall angles of attack. The frequency and strength of reaching total negative (reversed) deflections can indicate proximity to separation and stall

The time-series of tip deflections $Q_s(t)$ for pillars 1 to 6 (leading edge to trailing edge) were output and post-processed as outlined above. The mean deflection of the pillars $\overline{Q_s}$ alone was first considered for varying angles of incidence. Firstly, the mean deflection of the first pillar $\overline{Q_{s,1}}$ is seen to be largely unaffected by changes of angle of attack until separation, as changes in boundary layer thickness and profile have a negligible effect on the mean tip deflection of that pillar, lying nearer to the leading edge. This can be seen on the first data points of Fig. 8b and is illustrated more clearly in Fig. 8a.

Additionally, as the angle of attack changes so does the boundary layer chord-wise growth rate and profile, which has an effect on the mean bending of the pillars $\overline{Q_s}$. The effects of boundary layer changes on the deflection of flexible pillar structures have previously been investigated [4] and is seen herein by the results from both Figs. 2 and 8a. The relative tip deflection for pillars aft of the second pillar to the first pillar is therefore seen to increase as the angle of attack increases approaching stall. This allowed for a measure of instantaneous angle of attack by observing this relative deflection $\overline{Q_{s,N}} - \overline{Q_{s,1}}$. Seeing that the deflection of the first pillar is relatively unaffected by changes in angle of attack, while later pillars are clearly affected, allows for there to be an expected unique combination of total deflection of the leading-edge-most pillar and relative deflection of aft pillars, thus providing a reading of instantaneous free-stream velocity and angle of attack.

Moreover, it can be seen in Fig. 9 that the amplitude of fluctuations gets larger with chord-wise distance, eventually going into negative deflections, which occur more frequently at critical angles of attack immediate to stall. This is the footprint of growing instabilities in the flow.

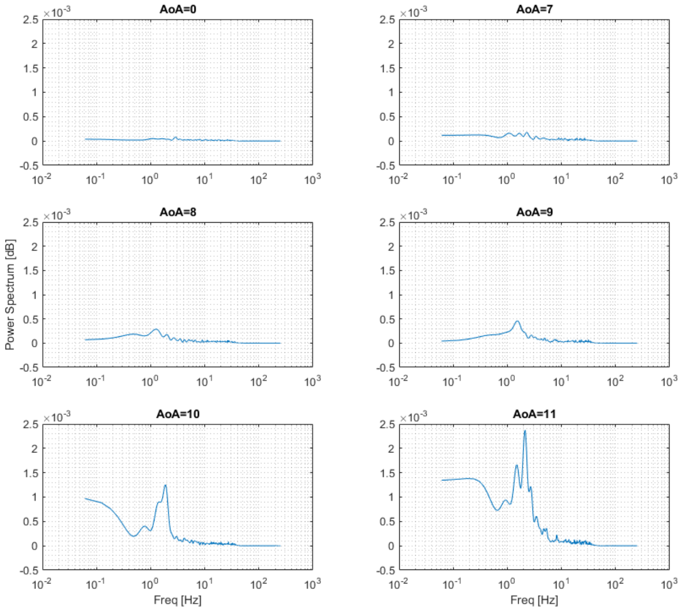

Fig. 10: Spectral analysis of pillar deflections at increasing angles of attack showing the increase in frequency and intensity of the low-frequency oscillations as stall is approached. The peaks for AoA's 8, 9, 10, and 11 correspond to Strouhal numbers of 0.016, 0.019, 0.024, and 0.027 respectively

Fig. 10 shows the result for an exemplary pillar at 45% chord from spectral analysis of the displacement values. This is done using the low-pass filtered time-series of pillar tip deflections to exclude peaks from the natural frequency oscillations. The results for an angle of incidence of 0° and 7° are included. These show no discernible peaks of notable strength. Low frequency oscillations start to be detected by this pillar at 8°, with a relatively weak peak beginning to form. With further growing AoA a dominant oscillation frequency emerges, which corresponds to a Strouhal number in the same order as the one found in previous research on incipient stall. Therefore the peak is hypothesised to be linked to quasi-periodic shear-layer flapping downstream of the laminar separation bubble.

What is noticed is that not only does the peak frequency increase with increase in angle of attack but also the peak strength varies markedly as the wing approaches stall. These are both quantities which can act as markers for instantaneous angle of attack sensing and indicators for incipient separation and stall. The Strouhal number of the most dominant oscillations for the angle of attack shows the trend for those pre-stall angles of attack where the low frequency oscillations appear (Fig. 10). These lie within the range of the low frequency oscillations observed by [7] and [8].

To investigate the validity of such markers for dynamic motions of the aerofoil, thus also indicating early incipient stall, the tests were run for ramp-up motion experiments with the aerofoil. In such a run the angle of incidence of the model was steadily changed from 0 to 15 degrees at a rate of (1.85 degrees/second), corresponding to a reduced frequency $k = 0.5 \times 10^{-3}$.

$$k = \frac{\rho \times f \times c}{U_{inf}} \tag{4}$$

Fig. 11 shows the original data and the results after low-pass filtering for each pillar. As the aerofoil approaches separation (approx. $5 - 6s$ or $9 - 11°$) similar low frequency oscillations to those in the steady aerofoil situation at higher AoA become pronounced. Therefore it is concluded that the detection of specific low-frequency oscillations in the above discussed Strouhal-number range is unique to incipient separation.

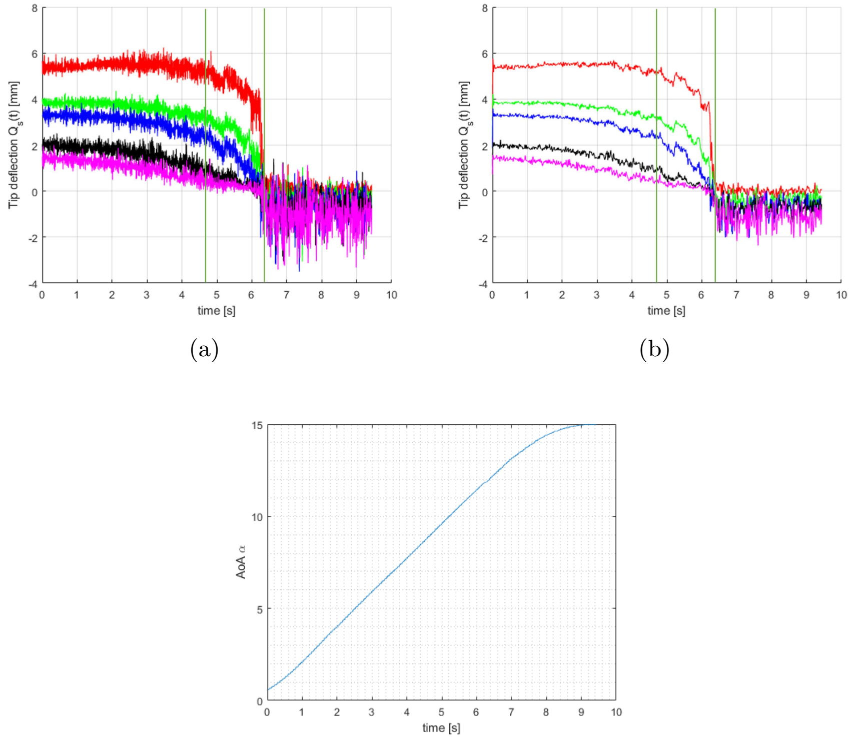

(a) (b)

(c)

Fig. 11: (a)Results from ramp-up study showing oscillation and pre-stall behaviour of pillar tip deflections. The low frequency oscillations appear at pre-stall angles (encircled) and are more apparent after low-pass filtering (right). Pillars no.1 to 5 shown in red, green, blue, black, and magenta respectively. (c) The incidence of the model from the ramp-up study was ramped up steadily from 0 degrees to 15 degrees in approximately 9 seconds

Additional flow field measurements were done using High-Speed Particle Image Velocimetry to further investigate the low-frequency oscillations. A virtual probe was put at a chord of 45% and 3mm wall distance to analyse the fluctuations in the streamwise velocity component. Fig. 12 shows the probe signal in the PIV results compared to the smoothed and filtered results from the third pillar from both the high-speed recordings and the object tracking camera recordings. The object tracking camera was trained on the central pillars to track tip deflections with a sampling rate of $250Hz$. The comparison of all three plots show striking similarity of low-frequency oscillations although the signals were not taken simultaneoues.

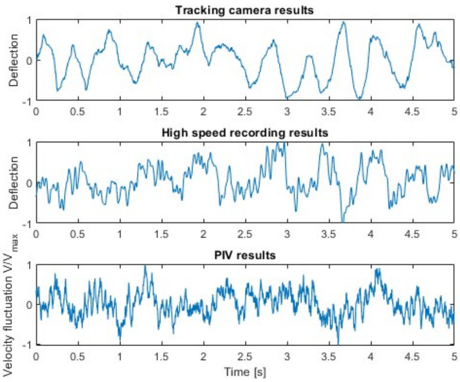

Fig. 12: Fluctuating component of deflection relative to the mean from the pillar placed at 45% chord are shown from 3 separate experiments, normalised with the maximum. (a) results from the object tracking camera, (b) from the processed images of the high-speed recording, and (c) from the streamwise velocity component at the probe location from the time-resolved PIV recordings, all at an AoA of 10 degrees.

4 Conclusions and outlook

This paper presents a series of results from experimental work on a NACA0012 aerofoil model using a system of flexible pillar sensors that emanate from the suction side of the aerofoil and are tracked optically acting as "digital tufts". These are monitored to give real-time high temporal resolution data that correlates with flow velocities from which frequencies of flow structures over the wing can be analysed. These data were used herein to identify underlying patterns that give rise to flow separation and stall. Such markers were found in the growth of amplitude in specific low-frequency oscillations, that are hypothesised as emanating from the laminar separation bubble for increasing AoA. Optical tracking of these sensors revealed their ability to detect those oscillations as pre-cursor to incipient stall.

For static conditions of the aerofoil, the time-averaged deflections of all pillars across the chord of the wing show a unique combination that is indicative of the instantaneous angle of attack prior to stall. That is, by observation of the trend of mean deflection of the sensors in downstream direction, which is represented by the gradient of the mean pillar deflections, it can be seen as unique to each angle of attack. This result is due to the variation of the boundary layer with chord and AoA and the resulting integration effect on the pillar sensors. The sensitivity of such type of sensor to the thickness and the shape factor of the boundary layer has been shown already in [4] and is confirmed herein by the observed results for varying angles of attack.

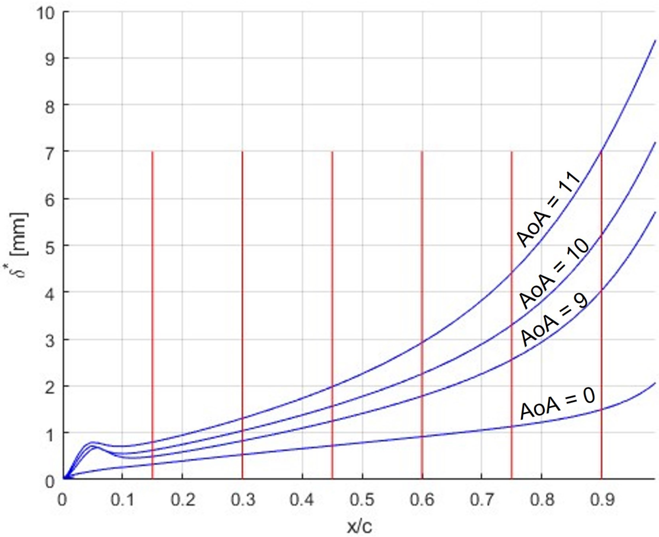

Fig. 13: Estimation of the displacement thickness as the angle of attack approaches stall, with reference to pillar position and length overlaid in red. Values of δ were obtained using xfoil [15]

By monitoring the fluctuating component of sensor deflection it was seen that the amplitude of fluctuations increases with AoA, particularly for the aft-most pillars, and eventually reaching negative deflections near critical angles of attack. Those fluctuations are related to growing instabilities, the most dominant one found at relative low Strouhal numbers for angles of attack as early as 8°. Such patterns either are known to correlate with known phenomena as herein concluded from previous detailed work on such aerofoils, or they could be found using training of artificial neural networks. Herein, previous data in literature let us hypothesise that the low-frequency oscillations are linked to the quasi-periodic breathing of the laminar separation bubble formed over the suction side of the wing. The frequency and intensity of such signature as tracked by the flexible pillar sensors can be correlated with the flight condition, specifically the angle of attack. Alternatively, other correlations can be tested for specific flight condition in training, or learnt from application to be identified by training a specialised neural network.

There is a general limitation with such hair-type sensor arrays, firstly the fact that those sensors are invasive to the flow and secondly that their dynamics may interfere with the output of one another, thus the pillars must be spaced apart appropriately to avoid interaction effects and to ensure that the reading from each pillar is representative of the surrounding flow conditions. That way, their readings can be considered collectively, as in Fig. 8b, or individually, as in Fig. 10 to provide flow conditions information.

The pillars were designed to balance between facilitating optical tracking from standard optical systems mounted on-board, while providing least possible disturbance to the flow. This is a trade-off between reducing the dimensions of the pillars such that their invasive character is reduced, and the resolution limit of the imaging system, where smaller structures lead to less visibility and lower optical resolution. The arrangement used herein together with the rather moderate Re-number flows tested herein represents a good practical compromise of the given system for the envisioned application of such sensors on small UAVs.

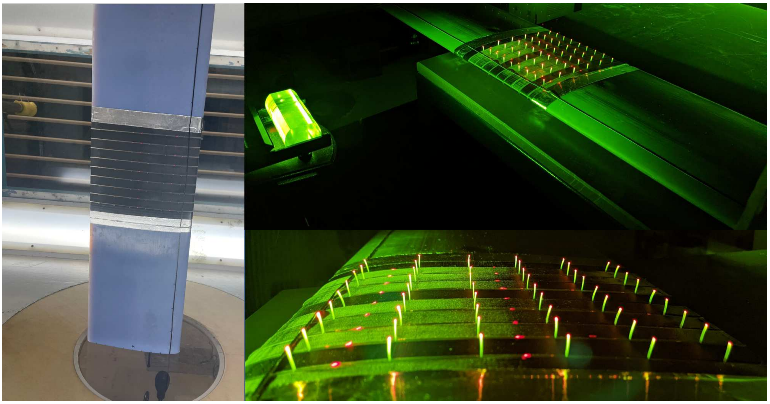

Fig. 14: Setup of experiment with array of sensors attached. The tips are illuminated with green LED light

The pillar sensors can provide a multitude of velocity and velocity-derived data to be used for real-time diagnostics. Compared to wool tufts visualisations, the pillar sensors capability to encode the mean and fluctuating part of the local velocity provides a more rich diagnostics of the current flow state. Spectral analyses of the "digital tufts" in conjunction with pattern recognition algorithms were used here to identify specific quantities unique to the flight conditions. Introducing and training a specialised neural network to identify the local flow conditions, such as was carried out with similar nature-inspired sensors in [10] is planned as further development of this system. Furthermore, spatial near-wall flow field recovery techniques can be applied from the relative sparse sensor placement using deep-learning. For timely decision making and response of the signals in an aeronautical system in-situ, the signals must be collected and processed "on the fly" with optical systems that can filter out irrelevant data using physical means such as wavelength separation, in addition to computational means, and then process that data within the required time period. Using the on-line object tracking it was possible to train the camera on the relevant pillar tips to instantaneously output a time-series of coordinates corresponding to the pillar tip deflections for a specified time period and sampling rate. These type of recordings with multiple levels of filtering and pre-processing often are affected by corrupt or sparse data. Emerging technologies in reconstructing such data structures such as sparse representation and compressive sensing can allow for the timely and efficient onboard processing of these data for subsequent flight or flow control decision making [16].

Finally, spanwise data can be obtained by including a 2D array of these pillar sensors over a wing. These can be used as "digital-tufts" over the skin of a wing in a wind-tunnel, or fitted onto the system in operation. Coherent signatures of flow events over several pillar sensor positions is a way to distinguish noise from relevant structures. Current work on the sensors is looking at local flow conditions at post-stall angles of attack as a way of characterising spanwise local stall phenomena simply from tip-deflection data of the pillars (Fig. 14). This, coupled with the developed signal processing from the sensors will allow the ability to provide diagnostic data for an aerodynamic system's performance over a wide regime of flow conditions. This leads into the development of a system of biologically inspired sensors which react in a predictable manner to changes in flow conditions within the flight regime of small to medium sized UAVs, which can be used in-situ to promptly provide diagnostic data to a flight control system, or can be used for diagnostics in experimental conditions.

Declarations

Ethical Approval. Not applicable

Authors' contributions. O. Selim conducted the experiments and simulations all under the supervision and advice of C. Bruecker. O. Selim and C. Bruecker conceptualised the study and analysed the data, and both authors wrote the manuscript.

Funding. The authors would like acknowledge and express their gratitude to the George Daniels Educational Trust, who fund the position of O. Selim, as well as BAE Systems and the Royal Academy of Engineering (grant RCSRF1617/4/11) for supporting the position of C. Bruecker,

Competing interests. The authors declare no competing interests.

Availability of data and materials. The datasets used and/or analysed during the current study available from the corresponding author on reasonable request.

Acknowledgements. The authors would also like acknowledge and express their gratitude to Deutsche Forschungsgemeinschaft (DFG) for their support with provision of some of the optical systems used in this study. Additionally, the authors would like to express thanks to Alecsandra Court for her role in the continuation and development of the pillar sensor arrays and Ibrahim Kejje for his diligent work on the development of the calibration wind tunnel.

References

[1] Mohamed, A., Watkins, S., Clothier, R., Abdulrahim, M., Massey, K., Sabatini, R.: Fixed-wing mav attitude stability in atmospheric turbulence—part 2: Investigating biologically-inspired sensors. Progress in Aerospace Sciences **71**, 1–13 (2014)

[2] Brücker, C., Schlegel, D., Triep, M.: Feather vibration as a stimulus for sensing incipient separation in falcon diving flight. Natural Resources **07**, 411–422 (2016)

[3] Selim, O., Gowree, E.R., Lagemann, C., Talboys, E., Jagadeesh, C., Brücker, C.: Peregrine falcon's dive: Pullout maneuver and flight control through wing morphing. AIAA Journal **59**(10), 3979–3987 (2021)

[4] Dickinson, B.T.: Hair receptor sensitivity to changes in laminar boundary layer shape. Bioinspiration & biomimetics **5**(1), 016002 (2010)

[5] Brücker, C., Bauer, D., Chaves, H.: Dynamic response of micro-pillar sensors measuring fluctuating wall-shear-stress. Experiments in fluids **42**(5), 737–749 (2007)

[6] Brücker, C.: Evidence of rare backflow and skin-friction critical points in near-wall turbulence using micropillar imaging. Physics of Fluids **27**(3), 031705 (2015)

[7] ElAwad, Y.A., ElJack, E.M.: Numerical investigation of the low-frequency flow oscillation over a naca-0012 aerofoil at the inception of stall. International Journal of Micro Air Vehicles **11**, 1756829319833687 (2019)

[8] Tanaka, H.: Flow visualization and piv measurements of laminar separation bubble oscillating at low frequency on an airfoil near stall. In: 24th International Congress of the Aeronautical Sciences, pp. 1–15 (2004)

[9] Li, Q., Stavropoulos-Vasilakis, E., Koukouvinis, P., Gavaises, M., Bruecker, C.H.: Micro-pillar sensor based wall-shear mapping in pulsating flows: In-situ calibration and measurements in an aortic heart-valve tester. Journal of Fluids and Structures **105**, 103346 (2021)

[10] Elshalakani, M., Muthuramalingam, M., Bruecker, C.: A deep-learning model for underwater position sensing of a wake's source using artificial seal whiskers. Sensors **20**(12), 3522 (2020)

[11] Oertel, H.: Prandtl's Essentials of Fluid Mechanics. Springer, ??? (2004)

[12] Gosselin, F.P., De Langre, E.: Drag reduction by reconfiguration of a poroelastic system. Journal of Fluids and Structures **27**(7), 1111–1123

(2011)

[13] Zheng, X., Yu-Bin, L., Pu, C., Feng, S., ZHANG, S.-J., Xiang-Rong, F.: Flutter frequency based on bending-torsion coupling theory. In: The 8th International Conference on Computational Methods (ICCM2017) (2017)

[14] Leclercq, T., de Langre, E.: Vortex-induced vibrations of cylinders bent by the flow. Journal of Fluids and Structures **80**, 77–93 (2018)

[15] Drela, M.: Xfoil: An analysis and design system for low reynolds number airfoils. In: Low Reynolds Number Aerodynamics, pp. 1–12. Springer, ??? (1989)

[16] Callaham, J.L., Maeda, K., Brunton, S.L.: Robust flow reconstruction from limited measurements via sparse representation. Physical Review Fluids **4**(10), 103907 (2019)